J. Fluid Mech. (1968), *vol.* 31, *part* 1, *pp.* 113–139
Printed in Great Britain

Large-amplitude Bénard convection in a rotating fluid

By GEORGE VERONIS

Department of Geology, Yale University, New Haven, Connecticut

(Received 16 June 1967)

Linear stability theory of Bénard convection in a rotating fluid (Chandrasekhar 1961) has shown that fluids with large ($\gg 1$) Prandtl number, σ, exhibit behaviour markedly different from that of fluids with $\sigma \ll 1$. This difference in behaviour extends also into the finite-amplitude range (Veronis 1959, 1966 I). In this paper we report a numerical study of two-dimensional Bénard convection in a rotating fluid confined between free boundaries, with $\sigma = 6{\cdot}8$ and $\sigma = 0{\cdot}2$ for the range of Taylor number $0 \leqslant \mathscr{T}^2 \leqslant 10^5$ and for Rayleigh numbers, R, extending an order of magnitude from the critical value of linear stability theory. The behaviour of water ($\sigma = 6{\cdot}8$) is dominated by the rotational constraint even for relatively moderate values ($\sim 10^3$) of $\mathscr{T}^2$. A study of the resultant velocity and temperature fields shows how rotation controls the system, with the principal behaviour reflected by the thermal wind balance; i.e. the horizontal temperature gradient is largely balanced by the vertical shear of the velocity component normal to the temperature gradient. A fluid with a small Prandtl number ($\sigma = 0{\cdot}2$) becomes unstable to finite-amplitude disturbances at values of the Rayleigh number significantly below the critical value of linear stability theory. The subsequent steady vorticity and temperature fields exhibit a structure which is quite different from that of fluids with large σ. The rotational constraint is balanced primarily by non-linear processes in a limited range of Taylor number ($\mathscr{T}^2 \leqslant 10^{3{\cdot}6}$). For larger values of $\mathscr{T}^2$ the system first becomes unstable to infinitesimal oscillatory disturbances but a steady, finite-amplitude flow is established at supercritical values of R which are none the less smaller than the values that one would expect from linear theory. The ranges of Taylor number in which the above phenomena occur are different from those which were estimated on the basis of an earlier study (Veronis 1966 I) which made use of a minimal representation of the finite-amplitude velocity and temperature fields. No subcritical, finite-amplitude oscillatory motions were found in the present study. Comparison with some of the experimental features observed and reported by Rossby (1966) is also discussed and it is pointed out that some of the differences between theory and experiment may be traced to the restrictive conditions (two-dimensionality and free boundaries) of the present study.

1. Introduction and summary

The study of the processes involved in two-dimensional Bénard convection is extended in this paper to include the effects of a uniform rotation of the fluid layer about a vertical axis. By means of an electronic computer it is possible to

consider flows of quite large amplitude and to investigate strong non-linear effects when rotation is present.

A preliminary analysis (Veronis 1966 I, hereafter referred to as I) with a severely truncated Fourier representation was made for a rotating convecting fluid bounded above and below by free surfaces. The principal result obtained is that finite-amplitude motions can exist at values, R_f, of the Rayleigh number, R, which

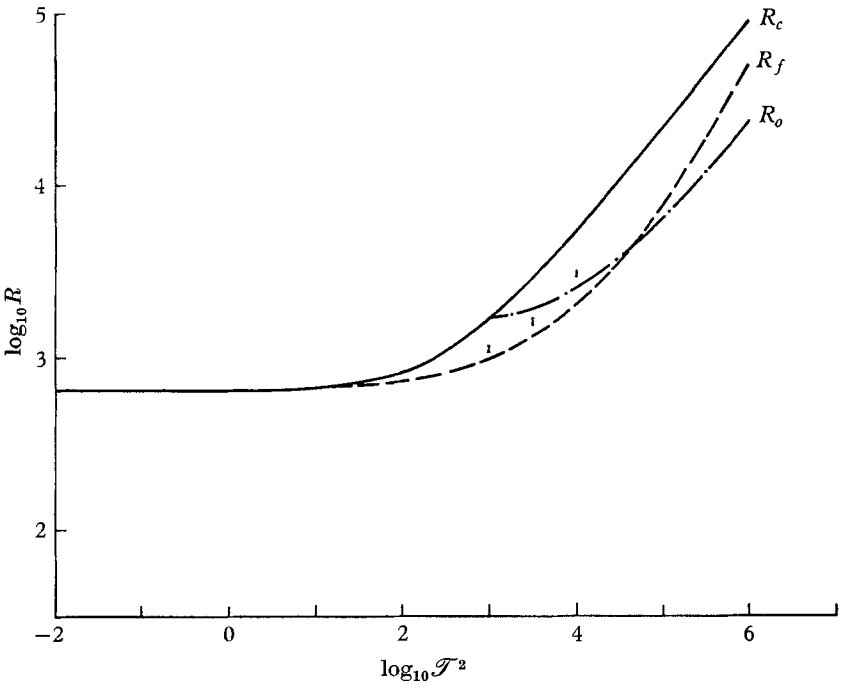

FIGURE 1. The minimum Rayleigh numbers at which motion can be marginally maintained are plotted as functions of $\mathscr{T}^2$ with $\sigma = 0{\cdot}2$. The solid and dash–dot curves show the values at which linear theory predicts exchange of stability (R_c) and overstability (R_o). The dashed curve (R_f) shows the lowest values of R at which finite-amplitude motions can be maintained according to the results from a minimal representation of the velocity and temperature fields. The present analysis predicts that at $\mathscr{T}^2 = 10^3$, $10^{3\frac{1}{2}}$ and 10^4 the minimum R for finite-amplitude instability will occur in the ranges designated by the small vertical lines.

were substantially lower than the values predicted by linear stability theory. For this result to hold it is necessary that the Prandtl number, σ, of the fluid be less than about $\sqrt{2}$ and the Taylor number, $\mathscr{T}^2$, lie in a restricted range.

In this paper we shall once again use a truncated Fourier representation but the number of terms is taken to be sufficiently large so that the results are not significantly altered by extending the representation. We follow the procedure used to study Bénard convection in a non-rotating fluid (Veronis 1966 II, hereafter referred to as II) to derive results for Rayleigh numbers extending an order of magnitude from the critical value.

Figure 1 may serve as an aid to delimit the scope of the present study. We show three curves of R *vs.* $\mathscr{T}^2$ for convection between free boundaries. The solid curve is a graph of R_c *vs.* $\mathscr{T}^2$, where R_c is the minimum value of the Rayleigh number

which can sustain infinitesimal, steady convection (Chandrasekhar 1961). The values of R_c are independent of the Prandtl number. The dash–dot curve is a plot of R_o *vs.* $\mathscr{T}^2$, where R_o is the minimum R for which infinitesimal, overstable (oscillatory) motions can exist when $\sigma = 0{\cdot}2$. Thus overstable modes, which occur in the range $\mathscr{T}^2 \geqslant 10^3$, can exist at values of R significantly lower than R_c. According to linear theory, therefore, the onset of convection should take the form of oscillatory motions.

The dashed curve shows the values of R_f *vs.* $\mathscr{T}^2$ for $\sigma = 0{\cdot}2$ where R_f is the minimum R at which finite-amplitude, *steady* motions can exist according to the analysis of I. Since R_f lies below both R_c and R_o, it is possible for *finite-amplitude* instability to occur provided that the system is disturbed appropriately.

It was pointed out in I that finite-amplitude instability occurs because non-linear effects can balance part of the constraint of rotation, thereby reducing the inhibiting effect of rotation on convecting motions. It is clearly necessary that $\mathscr{T}^2$ be sufficiently large for the constraint to be effective in order that the system be able to reduce the effect. Also, it is necessary that non-linear effects be sufficiently large to offset the effect of the constraint in order for finite-amplitude instability to occur. When $\mathscr{T}^2$ is large, the required intensity of non-linear effects must be so large that they cannot be generated at subcritical R so that, for sufficiently large $\mathscr{T}^2$, we find that $R_f > R_c$.

These qualitative conclusions of I were verified experimentally by Rossby (1966), who carried out an extensive investigation of Bénard convection of several fluids in both rotating and non-rotating frames. In his experiments with mercury Rossby observed a definite finite-amplitude instability in a limited range of Taylor number. However, the motions were always transient (even when the systems were non-rotating). In spite of this fact, he was able to separate the types of instability into those related to overstable modes (periodic, oscillatory behaviour) and other modes (aperiodic behaviour). The latter are presumably the ones predicted by our results since they are similar to those which Rossby observed in a non-rotating fluid at small supercritical R. In any event the qualitative features of our preliminary study have been verified.

It was not possible to extend the analytical methods of I to include time-dependent motions and part of the purpose of this numerical study was to see whether the subcritical oscillatory modes detected by Rossby would be exhibited by our numerical model.

The mathematical problem and some of the details of the validity of the Fourier representation and the numerical analysis are outlined in the next three sections. Section 5 contains a discussion of the results when the fluid has a Prandtl number of 6·8 (the value of σ for water at room temperature). According to the analytical results of I, fluids with $\sigma > \sqrt{2}$ should not exhibit finite-amplitude instability so in this sense the results with $\sigma = 6{\cdot}8$ can be interpreted as characteristic of fluids with large Prandtl number.

Quantitative results of heat flux (in the form of Nusselt number, Nu) *vs.* R are given in §5 for $\sigma = 6{\cdot}8$ and for $\mathscr{T}^2 = 10^3$, 10^4 and 10^5. The increasingly strong constraining effects of rotation are reflected in several features of the flow. Linear theory predicts that the critical Rayleigh number increases as $\mathscr{T}^2$ increases. The

numerical integrations show that at low rotation rates ($\mathscr{T}^2 \leqslant 10^3$) the thermal field exhibits a structure similar to that of a non-rotating fluid with anvil-shaped plumes of warm (cold) fluid extending to the upper (lower) boundary. When $\mathscr{T}^2$ is increased to 10^5 the horizontal spreading of warm (cold) fluid near the upper (lower) boundary is inhibited. Flow does not take place down the pressure gradient but instead horizontal temperature gradients are balanced by the vertical shear of the zonal velocity, v. This so-called thermal wind balance (in the vertical vorticity equation horizontal temperature gradients are balanced by vertical shear, i.e. by the Coriolis terms) is characteristic of stratified fluids which are dominated by rotation.

If the constraint is very effective, i.e. if the horizontal temperature gradient is largely balanced by the vertical shear of the zonal velocity, then the latter should reflect this balance through the symmetry of its horizontal distribution. This behaviour is exhibited in figures 5*a* and 5*b* which show contour lines of the zonal velocity which are nearly symmetric about the mid-point of a cell and in figure 6 which shows the horizontal structure of the vertical average, v_m, of the zonal velocity. In the latter figure v_m is nearly antisymmetric about the mid-points of each half-cell. Since v_m is a measure of the intensity of the non-linear processes, the symmetry properties provide us with the information that the primary structure of the zonal velocity, v, is directly attributable to the horizontal structure of the temperature field. The slight skewness exhibited by the zonal velocity and its vertical integral reflect non-linear processes which are not a direct consequence of the thermal wind balance.

To get a better picture of the type of balance which may exist when the thermal wind relation is not dominant we turn to the corresponding results for a fluid with low Prandtl number ($\sigma = 0{\cdot}2$). Figures 11*a* and 11*b* show contour lines of v in the vertical plane. The near-symmetry which is evident in figure 5*a* and *b* is no longer present and the zonal velocity is intensely concentrated in the lower left- and upper right-hand regions of the cell. This type of structure is characteristic of a fluid in which the Coriolis force is balanced primarily by non-linear or inertial accelerations. Figure 12 shows that v_m is no longer antisymmetric within each half-cell, i.e. v_m does not simply reflect the forced non-linear harmonics of a basic thermal wind balance.

Another difference in the response of fluids with large and small Prandtl numbers is evident from a comparison of the results of Nu *vs.* R for $\sigma = 6{\cdot}8$ (table 1) and $\sigma = 0{\cdot}2$ (tables 3–5). Qualitatively a fluid with large Prandtl number behaves in a manner similar to that of a non-rotating fluid; i.e. after the point of instability according to linear theory the heat flux increases with increasing R. When σ is small, the fluid may sustain strong finite-amplitude motions at subcritical values of R.

As we mentioned earlier, this possibility of finite-amplitude instability for fluids with $\sigma < \sqrt{2}$ was derived in I. The extent to which that result is verified by an accurate representation is seen in figure 1, where the small vertical lines at $\mathscr{T}^2 = 10^3$, $10^{3\frac{1}{2}}$ and 10^4 show the ranges of Rayleigh number within which finite-amplitude steady motions could first be maintained according to the present calculations. Thus the fluid will exhibit finite-amplitude instability

in more restricted ranges of Taylor and Rayleigh numbers than are predicted by the severely truncated representation of I.

Linear theory predicts that instability will take the form of oscillatory motions for sufficiently small σ (Chandrasekhar 1961). In this study we find that part of the range of Taylor numbers for which these oscillatory modes should occur first is pre-empted by finite-amplitude instability (see figure 1), although this range too is more restricted than the one predicted in I. According to that study $R_f < R_o$ for $\mathscr{T}^2 \leqslant 10^{4\cdot5}$. Now we find that finite-amplitude motions may occur first only in the range $\mathscr{T}^2 \leqslant 10^{3\cdot6}$. However, in the present calculations it was also found that even when $\mathscr{T}^2 > 10^{3\cdot6}$ finite-amplitude steady motions occur in the range $R_o < R < R_c$. Hence, the system is still unstable to steady finite-amplitude disturbances although an instability to infinitesimal oscillatory motion is the first to occur.

Two numerical integrations have shown that, where instability to infinitesimal oscillatory modes is the first to occur, non-linear processes alter the period of the oscillation somewhat although the change is small (figure 8). As the Rayleigh number is increased from the value R_o, a skewness in the plot of Nu *vs.* time reflects the influence of non-linearities on the simple periodic (harmonic) structure of the oscillation.

Several of the phenomena observed by Rossby (1966) were not encountered in this study. These include subcritical, steady, finite-amplitude motions in water and subcritical oscillatory modes in mercury. The former was explained by Rossby as the result of the relaxation of rigid boundary conditions by Ekman layers which form near the boundaries of a rotating fluid confined between rigid plates. Thus, according to Rossby, the relaxation of the rigid boundary conditions enables the fluid to convect as if it were confined between (less constraining) free boundaries.

In none of the present calculations did subcritical oscillatory motions occur. This may be due to the fact that the analysis is based on a two-dimensional model with a single basic wave-number. The relaxation of these two conditions plus the inclusion of rigid boundaries admits so many alternative possibilities to the fluid that the behaviour may well be quite different from what we have derived.

In our study with $\sigma = 0{\cdot}2$ we used maximum heat flux (or maximum Nusselt number, which we shall denote as $Nu_{\max}$) to determine the wave-number, α, which is presumably preferred in convection. The Nusselt number depends only mildly on α in a non-rotating fluid (for the range of R considered) and a similar dependence is observed in the weakly rotating system ($\mathscr{T}^2 \leqslant 10^3$). However, for larger values of $\mathscr{T}^2$ it was found that the 'preferred' wave-number is strongly a function of R. The boxed values in tables 4 and 5 are those giving $Nu_{\max}$ as a function of α at each value of R shown. Thus in table 5 we note that, as R increases, the value of α corresponding to $Nu_{\max}$ decreases from 0·95 to 0·8. Now, if the fluid tends to choose that horizontal scale which gives $Nu_{\max}$, it is clear that the cell size must change gradually as R increases. This means that it may be difficult for a steady-state flow to be established since the scale of the flow is not firmly set and small variations in experimental conditions may be accompanied by adjustments in structure.

In his experiments with water Rossby observed that at a fixed Rayleigh number a maximum amount of heat is transported at a finite value of the Taylor number. This behaviour is somewhat surprising in view of the constraining effect of rotation. Rossby's explanation of this phenomenon is again that the presence of rotation allows Ekman boundary layers to form which then serve to relax the rigid boundary conditions for the bulk of the fluid so that the fluid 'sees' free boundaries. We encountered no such behaviour in these numerical calculations with free boundaries.

2. Equations

The lower boundary ($z = 0$) of the layer of fluid is maintained at temperature T_0 and the temperature of the upper boundary ($z = d$) is $T_0 - \Delta T$. We write the total temperature as

$$T_{\text{total}} = T_0 - \Delta T(z/d) + T(x, z, t), \tag{2.1}$$

where $T(x, z, t)$ is the deviation of the temperature from the linear profile.

Then the equations (all variations with respect to y are assumed to vanish) are the two-dimensional Boussinesq equations for the conservation of momentum

$$\partial \mathbf{v}/\partial t + \mathbf{v}.\nabla \mathbf{v} + 2\boldsymbol{\Omega} \times \mathbf{v} = -\rho_0^{-1} \nabla p - \mathbf{g}\rho'/\rho_0 + \nu \nabla^2 \mathbf{v}, \tag{2.2}$$

the conservation of mass

$$\partial u/\partial x + \partial w/\partial z = 0, \tag{2.3}$$

the linear equation of state for the fluctuation density

$$\rho' = -\rho_0 \alpha T, \tag{2.4}$$

and the equation for the conservation of heat

$$\partial T/\partial t - w(\Delta T/d) + \mathbf{v}.\nabla T = \kappa \nabla^2 T. \tag{2.5}$$

Here, $\mathbf{v}$ is the three-dimensional velocity vector with components (u, v, w) in the respective directions (x, y, z); $\boldsymbol{\Omega}$ is the constant rate of rotation of the entire system about the vertical (z) axis; g is the gravitational acceleration in the negative z-direction; ρ_0 is the density at temperature T_0; α is the coefficient of thermal expansion; and ν and κ are respectively the coefficients of kinematic viscosity and thermometric diffusivity. In equation (2.5) the linear part of T_{total} has been separated out and appears as the second term.

We cross-differentiate the first and third equations of motion in order to eliminate the pressure p. Then, defining the y-component of vorticity as

$$\eta = \partial u/\partial z - \partial w/\partial x, \tag{2.6}$$

we have

$$\partial \eta/\partial t + \mathbf{v}.\nabla \eta - 2\Omega(\partial v/\partial z) = -g\alpha(\partial T/\partial x) + \nu \nabla^2 \eta. \tag{2.7}$$

The second equation of motion has the form

$$\partial v/\partial t + \mathbf{v}.\nabla v + 2\Omega u = \nu \nabla^2 v. \tag{2.8}$$

We introduce the streamfunction, ψ, through the definitions

$$u = \partial \psi/\partial z, \quad w = -\partial \psi/\partial x, \tag{2.9}$$

so that
$$\eta = \partial u/\partial z - \partial w/\partial x = \nabla^2\psi. \tag{2.10}$$

Our system then becomes

$$\frac{\partial \eta}{\partial t} = J(\psi, \eta) + 2\Omega \frac{\partial v}{\partial z} - g\alpha \frac{\partial T}{\partial x} + \nu\nabla^2\eta, \tag{2.11}$$

$$\frac{\partial v}{\partial t} = J(\psi, v) - 2\Omega \frac{\partial \psi}{\partial z} + \nu\nabla^2 v, \tag{2.12}$$

$$\frac{\partial T}{\partial t} = J(\psi, T) - \frac{\Delta T}{d}\frac{\partial \psi}{\partial x} + \kappa\nabla^2 T, \tag{2.13}$$

where J stands for the Jacobian. Furthermore, the system is non-dimensionalized by

$$v = (\kappa/d)\, v', \quad t = (d^2/\kappa)\, t', \quad (x, z) = d(x', z'), \quad T = (\Delta T)\, T', \tag{2.14}$$

where the primed quantities are non-dimensional. Then equations (2.11) to (2.13) become

$$\partial\eta/\partial t = J(\psi, \eta) + \sigma\mathscr{T}(\partial v/\partial z) - \sigma R(\partial T/\partial x) + \sigma\nabla^2\eta, \tag{2.15}$$

$$\partial v/\partial t = J(\psi, v) - \sigma\mathscr{T}(\partial\psi/\partial z) + \sigma\nabla^2 v, \tag{2.16}$$

$$\partial T/\partial t = J(\psi, T) - \partial\psi/\partial x + \nabla^2 T, \tag{2.17}$$

where all of the variables are now non-dimensional, the primes have been dropped and the following non-dimensional parameters appear:

$$\left.\begin{aligned} &\text{Prandtl number, } \sigma = \nu/\kappa; \\ &\text{Taylor number, } \mathscr{T}^2 = 4\Omega^2 d^4/\nu^2; \\ &\text{Rayleigh number } R = g\alpha\, \Delta T\, d^3/\kappa\nu. \end{aligned}\right\} \tag{2.18}$$

The boundary conditions are based on the assumption that the boundaries at $z = 0$, 1 are perfect conductors of heat and are flat and stress-free. Then the conditions are

$$\frac{\partial v}{\partial z} = 0, \quad \psi = 0, \quad \frac{\partial^2\psi}{\partial z^2} = 0, \quad T = 0, \quad \text{on} \quad z = 0, 1. \tag{2.19}$$

3. Representation

We have assumed two-dimensional motions with a basic horizontal wavenumber denoted by α. Then a general spatial represention which satisfies the boundary conditions is

$$\left.\begin{aligned} \psi &= \sum_{m=1}^{M}\sum_{n=1}^{N} a_{mn} \sin(m\pi\alpha x) \sin(n\pi z), \\ T &= \sum_{m=0}^{M}\sum_{n=1}^{N} b_{mn} \cos(m\pi\alpha x) \sin(n\pi z), \\ v &= \sum_{m=1}^{M}\sum_{n=0}^{N} c_{mn} \sin(m\pi\alpha x) \cos(n\pi z), \end{aligned}\right\} \tag{3.1}$$

where the a_{mn}, b_{mn}, c_{mn} are generally functions of time. This representation is composed of the eigenfunctions of the linear stability problem and if M and N are allowed to become infinite the representation is a complete orthogonal set. In our treatment we shall truncate the sums by choosing finite values of M and N so that the representation will be only approximate. The accuracy of the results will be examined in connexion with specific solutions in the following sections.

If expressions (3.1) are substituted into equations (2.15) to (2.17) and if we multiply these equations respectively by $\sin(p\pi\alpha x)\sin(q\pi z)$, $\cos(p\pi\alpha x)\sin(q\pi z)$ and $\sin(p\pi\alpha x)\cos(q\pi z)$ and integrate from $x = 0$ to $x = 1/\alpha$ and $z = 0$ to $z = 1$, we derive the following sets of ordinary, non-linear, differential (in time) equations for the amplitudes of the harmonic components:

$$\begin{aligned}
\dot{a}_{pq} = &-\sigma\pi^2(p^2\alpha^2+q^2)\,a_{pq} - \frac{\sigma R\alpha p}{\pi(p^2\alpha^2+q^2)}\,b_{pq} + \frac{\sigma\mathscr{T} q}{\pi(p^2\alpha^2+q^2)}\,d_{pq} \\
&+ \frac{\pi^2\alpha}{4(p^2\alpha^2+q^2)}\Bigg\{\sum_{m=1}^{p-1}\sum_{n=1}^{q-1}(mq-np)\,[(p-m)^2\alpha^2+(q-n)^2]\,a_{mn}a_{p-m,\,q-n} \\
&+ \sum_{m=p+1}^{M}\sum_{n=q+1}^{N}(mq-np)\,[(p-m)^2\alpha^2+(q-n)^2-(m^2\alpha^2+n^2)]\,a_{m-p,\,n-q}a_{mn} \\
&+ \sum_{m=p+1}^{M}\sum_{n=1}^{q-1}[p(n-q)+mq]\,[m^2\alpha^2+(q-n)^2]\,a_{m-p,\,n}a_{m,\,q-n} \\
&+ \sum_{m=p+1}^{M}\sum_{n=q+1}^{N}[q(m-p)+np]\,[(m-p)^2\alpha^2+n^2-(m^2\alpha^2+(n-q)^2)] \\
&\qquad\qquad \times a_{m,\,n-q}a_{m-p,\,n} \\
&+ \sum_{m=p+1}^{M}\sum_{n=1}^{q-1}(np-mq)\,[(m-p)^2\alpha^2+(p-n)^2]\,a_{mn}a_{m-p,\,q-n} \\
&+ \sum_{m=1}^{p-1}\sum_{n=q+1}^{N}[p(q-n)-mq]\,[(p-m)^2\alpha^2+n^2]\,a_{m,\,n-q}a_{p-m,\,n} \\
&+ \sum_{m=1}^{p-1}\sum_{n=q+1}^{N}(np-mq)\,[(p-m)^2\alpha^2+(n-q)^2]\,a_{mn}a_{p-m,\,n-q}\Bigg\}, \qquad (3.2)
\end{aligned}$$

$$\begin{aligned}
\dot{b}_{pq} = &-\pi^2(p^2\alpha^2+q^2)\,b_{pq} - \pi\alpha p a_{pq} \\
&+ (1-\tfrac{1}{2}\delta_{p0})\,\frac{\pi^2\alpha}{4}\Bigg\{\sum_{m=0}^{p-1}\sum_{n=1}^{q-1}(np-mq)\,a_{p-m,\,q-n}b_{mn} + \sum_{m=p}^{M}\sum_{n=q+1}^{N}(np-mq) \\
&\qquad\qquad \times a_{mn}b_{m-p,\,n-q} \\
&+ \sum_{m=p+1}^{M}\sum_{n=q+1}^{N}[p(q-n)-mq]\,a_{m-p,\,n}b_{m,\,n-q} + \sum_{m=p}^{M}\sum_{n=q+1}^{N}[p(q-n)-mq] \\
&\qquad\qquad \times a_{m,\,n-q}b_{m-p,\,n} \\
&+ \sum_{m=p+1}^{M}\sum_{n=q+1}^{N}(np-mq)\,a_{m-p,\,n-q}b_{mn} + \sum_{m=0}^{p-1}\sum_{n=q+1}^{N}[p(n-q)+mq] \\
&\qquad\qquad \times a_{p-m,\,n}b_{m,\,n-q} \\
&+ \sum_{m=0}^{p-1}\sum_{n=q+1}^{N}(mq-np)\,a_{p-m,\,n-q}b_{mn} + \sum_{m=p}^{M}\sum_{n=1}^{q-1}[q(m-p)+np]\,a_{m,\,q-n}b_{m-p,\,n} \\
&+ \sum_{m=p+1}^{M}\sum_{n=1}^{q-1}(mq-np)\,a_{m-p,\,q-n}b_{mn}\Bigg\}, \qquad (3.3)
\end{aligned}$$

$$\dot{d}_{pq} = -\sigma\mathscr{T}\pi q a_{pq} - \sigma\pi^2(p^2\alpha^2+q^2)\,d_{pq}$$
$$-\frac{\pi^2\alpha}{4}(1-\tfrac{1}{2}\delta_{p0})\Bigg\{\sum_{m=1}^{p-1}\sum_{n=0}^{q-1}(qm-pn)\,a_{p-m,q-n}d_{mn}+\sum_{m=1}^{p-1}\sum_{n=q}^{N}[p(n-q)+mq]\times a_{p.m,n}d_{m,n-q}$$
$$+\sum_{m=1}^{p-1}\sum_{n=q+1}^{N}(pn-qm)\,a_{p-m,n-q}d_{mn}+\sum_{m=p+1}^{M}\sum_{n=0}^{q-1}(pn-qm)\,a_{m-p,q-n}d_{mn}$$
$$+\sum_{m=p+1}^{M}\sum_{n=0}^{q-1}[q(m-p)+np]\,a_{m,q-n}d_{m-p,n}+\sum_{m=r+1}^{M}\sum_{n=q}^{N}[q(p-m)-np]\times a_{m-p,n}d_{m,n-q}$$
$$+\sum_{m=p+1}^{M}\sum_{n=q+1}^{N}(qm-pn)\,a_{m-p,n-q}d_{mn}+\sum_{m=p+1}^{M}\sum_{n=q}^{N}(qm-pn)\,a_{nm}d_{m-p,n-q}$$
$$+\sum_{m=p+1}^{M}\sum_{n=q+1}^{N}[p(q-n)-qm]\,a_{m,n-q}d_{m-p,n}\Bigg\}, \tag{3.4}$$

where p and q have the same range as in (3.1) and δ_{ij} is the Kronecker delta. The overdot on the left-hand side of each equation denotes a time derivative.

4. Numerical procedure

Equations (3.2) to (3.4) must be integrated in time so that a suitable set of initial conditions must be given. Experience with the non-rotating system (see II) showed that, when the system is unstable to supercritical disturbances only and when the solution is steady, the final solution is independent of the initial conditions. In the present investigation the same procedure proved to be valid for those cases with $\sigma = 6.8$. Hence, since we can derive an analytical solution for the system truncated with $M = N = 2$ (see I), we have used this solution as a starting-point for systems with $M > 2$, $N > 2$ because convergence is achieved most rapidly when the initial conditions approximate the final solution.

When $\sigma = 0{\cdot}2$, motions can occur for subcritical R. In this case the initial conditions are important because a disturbance composed of 'infinitesimal' values decays (that is what is meant by the term, subcritical). Hence, it is necessary that the initial conditions be appropriate to give rise to instability where the latter is possible. In most runs it sufficed to take as initial conditions the analytical results obtained with $M = N = 2$. However, it is possible that *oscillatory* motions can exist at values of R smaller than those for which finite-amplitude steady motions exist. To investigate this possibility at low values of R we took as initial conditions the solution (either steady or oscillatory) which existed for larger values of R. When it leads to maintained motions, this procedure is sufficient to prove finite-amplitude instability. When the motion decays, we call the system stable. It is obvious that we have not proved general stability by this procedure and the term 'stable' should be interpreted accordingly.

As in II we choose a maximum number of modes, K, and calculate all components and all interactions such that $M+N \leqslant K$ and $0 \leqslant p = M$, $0 \leqslant q \leqslant N$. This procedure allows the largest systems which consistently take into account all interactions up to any given order. Also, as in the earlier work we take into

account only those components such that $m+n$ is even, because a few runs including the terms with $m+n$ odd showed that the latter always decayed. Systems with $K = 4$, 6, 8 and 10 were treated.

Physical information of interest to us is the value of the Nusselt number, Nu, as a function of R. The Nusselt number is defined as the ratio of the vertical heat flux, H, to the conductive vertical heat flux. In the steady state the vertical heat flux is independent of the vertical co-ordinate, z, and can be evaluated as

$$H = -\kappa \left\langle \frac{\partial}{\partial z} T_{\text{total}} \right\rangle_{z=0}, \tag{4.1}$$

where the angular brackets correspond to a horizontal average. Using (3.1) we can rewrite (4.1) as

$$H = \kappa \frac{\Delta T}{d} - \kappa \frac{\Delta T}{d} \sum_{n=1}^{N} n\pi b_{0n}. \tag{4.2}$$

Hence Nu can be written as

$$Nu = \frac{Hd}{\kappa \Delta T} = 1 - \pi \sum_{n=1}^{N} n b_{0n}. \tag{4.3}$$

For time-dependent motions H as defined by (4.1) can be interpreted only as the heat flux through the lower boundary since the heat flux may vary with z. However, we can still use Nu to describe the oscillatory behaviour, e.g. to deduce the period of the oscillation.

An efficient method of integrating equations (3.2) to (3.4) is the following: symbolically the equations can be written as

$$\dot{f} = F(f), \tag{4.4}$$

where f stands for the vector making up the different variables and $F(f)$ represents the right-hand sides of (3.2) to (3.4). Equation (4.4) is approximated by the implicit finite-difference form

$$f^{\tau+1} = f^{\tau} + \tfrac{1}{2}\Delta T[F(f^{\tau+1}) + F(f^{\tau})], \tag{4.5}$$

where $f^{\tau+1}$ is the value of f at $t = (\tau+1)\Delta T$ and ΔT is a time increment.

Because of the complicated form that $F(f)$ has, it is not generally possible to derive an explicit solution to (4.5). Hence, we get an approximate solution by the following iterative procedure:

$$f_0^{\tau+1} = f^{\tau} + \Delta T F(f^{\tau}), \tag{4.6a}$$

$$f_{n+1}^{\tau+1} = f^{\tau} + \tfrac{1}{2}\Delta T[F(f^{\tau}) + F(f_n^{\tau+1})], \tag{4.6b}$$

and let $f^{\tau+1} = f_{n+1}^{\tau+1}$ when $\quad |f_{n+1}^{\tau+1} - f_n^{\tau+1}| < 0{\cdot}01\Delta T.$ (4.7)

When ΔT is chosen optimally, the average number of iterations per time step is less than three.

For those cases in which a steady state was achieved the latter was considered to have been established when

$$|f^{\tau+1} - f^{\tau}| < 0{\cdot}01\Delta T \tag{4.8}$$

for each of the Fourier coefficients. This criterion yielded a Nusselt number constant to 5 significant figures.

The values of Nu depended on the size of the representation, i.e. on the value of K. As in II, we consider that a system is sufficiently well represented when successive values of K yield Nusselt numbers which differ by less than 1 %. In some of the runs it was not possible to achieve this degree of convergence. However, by examining the results with different values of K it was sometimes possible to estimate the probable error of the system with $K = 10$, the largest that was treated.

5. Results with large Prandtl number

Water has a Prandtl number, σ, of 6·8. According to linear stability theory, rotating fluids with a Prandtl number larger than unity cannot support overstable oscillations. Furthermore, analytical results with $K = 2$ (I) show that no subcritical finite-amplitude motions exist for the system with free boundaries. We expect, therefore, that only steady finite-amplitude convection will occur and no maintained motions can exist for $R < R_c$.

Calculations have been made with $\sigma = 6{\cdot}8$ for Taylor numbers of 10^3, 10^4 and 10^5. Linear stability theory for these cases yields the following results for the minimum critical Rayleigh number, R_c, and the associated value of the wavenumber, α, for the first two unstable modes:

$\mathscr{T}^2$	R_c (1st mode)	α (1st mode)	R_c (2nd mode)	α (2nd mode)
10^3	1676·12	1·18107	12300·0	1·57727
10^4	5377·14	1·81372	22158·3	2·16974
10^5	21309·0	2·74601	66249·2	3·32517

In table 1 we list values of Nu at these three different Taylor numbers for Rayleigh numbers ranging from R_c up to approximately $10R_c$. Values are given for different values of K so that one can estimate both the accuracy and the validity of the results.

With $\mathscr{T}^2 = 10^3$ the computed values of Nu are acceptable up to $R = 20{,}000$ with $K = 8$ and one can expect that $K = 10$ will give acceptable results for even larger R. Thus, these heat flux results are accurate up to about $15R_c$. The range of Rayleigh numbers for which we have acceptable results is somewhat smaller when $\mathscr{T}^2 = 10^4$. At $R = 50{,}000$ (less than $10R_c$) Nu calculated with $K = 10$ differs by more than 2 % from the value calculated with $K = 8$. Hence, we cannot accept results with $K = 10$ much beyond $R = 50{,}000$.

When $\mathscr{T}^2$ is increased to 10^5, we find that the range of R for which the heat fluxes satisfy the acceptability criterion is considerably more restricted. By $R = 100{,}000$ (less than $5R_c$) the values of Nu for $K = 8$ and $K = 10$ differ by more than 2 % and the disparity increases to more than 5 % by $R = 200{,}000$ ($< 10R_c$). Hence, our calculated values with $K = 10$ are acceptable only up to about $R = 100{,}000$.

These ranges of accurate results reflect a characteristic behaviour of the rotating system. Linear stability theory yields values of the Rayleigh number for which the fluid becomes unstable to disturbances consisting of a single cell in

$\mathscr{T}^2 = 10^3$ ($R_c = 1676$)				$\mathscr{T}^2 = 10^4$ ($R_c = 5377$)				$\mathscr{T}^2 = 10^5$ ($R_c = 21309$)			
	$K = 6$	$K = 8$	$K = 10$	R	$K = 6$	$K = 8$	$K = 10$	R	$K = 6$	$K = 8$	K
0	1·028	—	—	6,000	1·221	—	—	25,000	1·340	1·340	
0	1·139	—	—	8,000	1·813	—	—	35,000	2·193	2·199	2
0	1·342	—	—	10,000	2·289	—	—	50,000	3·172	3·234	3
0	2·520	—	—	15,000	3·125	3·141	—	75,000	4·138	4·351	4
0	2·866	—	—	20,000	3·664	3·714	3·722	100,000	4·674	5·025	5
0	3·471	3·479	3·481	25,000	4·041	4·136	4·152	150,000	5·248	5·796	6
0	3·898	3·928	3·934	30,000	4·332	4·469	4·497	200,000	5·561	6·248	6
0	4·497	4·602	4·617	40,000	4·754	4·983	5·045	—	—	—	
0	4·917	5·123	5·165	50,000	5·044	5·381	5·489	—	—	—	

TABLE 1. Values of Nu with $\sigma = 6{\cdot}8$ for different values of K at $\mathscr{T}^2 = 10^3$, 10^4, 10^5. Calculations were made with α corresponding to the minimum value of R_c as listed in the text.

the vertical (1st mode), to disturbances consisting of two cells in the vertical (2nd mode), etc. Values for the first and second mode are listed above and we see that the ratio of the critical Rayleigh number of the second mode to that of the first decreases with increasing Taylor number. With $\mathscr{T}^2 = 0$ the ratio is 16.

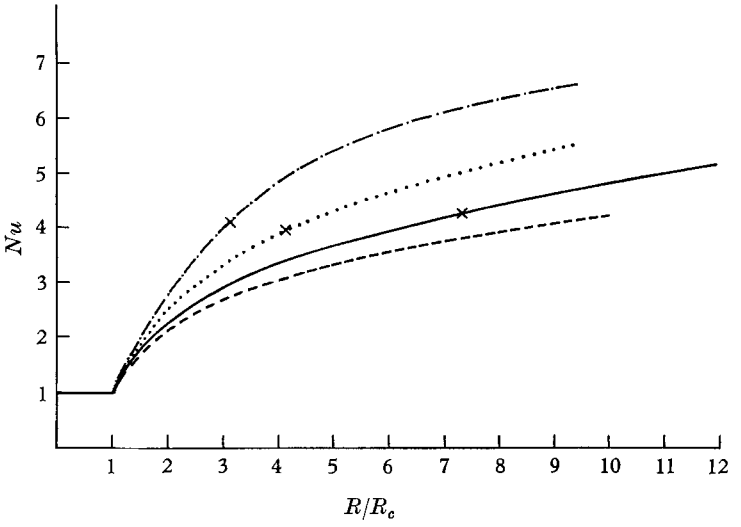

FIGURE 2. Nu *vs.* R/R_c for $\sigma = 6{\cdot}8$ and for a range of values of $\mathscr{T}^2$. The crosses on the curves with $\mathscr{T}^2 = 10^3, 10^4$ and 10^5 mark the values of R/R_c at which linear theory predicts instability to the second mode. At these points $Nu \approx 4$ for all three curves. —·—·, $\mathscr{T}^2 = 10^5$; ....., $\mathscr{T}^2 = 10^4$; ——, $\mathscr{T}^2 = 10^3$; – – – –, $\mathscr{T}^2 = 0$.

At $\mathscr{T}^2 = 10^3$ the ratio is 7·3. By $\mathscr{T}^2 = 10^5$ it has dropped to 3·11. Asymptotically as $\mathscr{T}^2 \to \infty$ the ratio approaches a value of 2·53. This decreasing ratio means that higher modes can become significant at relatively smaller values of the Rayleigh number because the increased structure associated with the higher modes becomes important sooner. It is evident that finer horizontal structure must also become important and therefore the size of the representation must increase.

In figure 2 we exhibit the data of table 1 in the form of a graph of Nu *vs.* R/R_c. Included for reference is the graph for $\mathscr{T}^2 = 0$ from the data in II. It will be noted that at any given value of R/R_c the Nusselt number increases with increasing $\mathscr{T}^2$. This behaviour is consistent with the remarks made in the preceding paragraph. The cross which appears on each of the curves $\mathscr{T}^2 = 10^3$, 10^4, 10^5 corresponds to the value of R at which instability of the second mode occurs according to linear stability theory. It will be noted that the Nusselt numbers at these values of R cluster around the value $Nu = 4$. This provides evidence that the heat flux for Bénard convection in a rotating fluid may be best described in terms of the range of Rayleigh numbers lying between the critical values of the different modes of linear stability theory.

As in the non-rotating system the field of streamlines in all computed cases shows that the motion is dominated by a single intense cell with no boundary layer. A typical case is shown in figure 3. There is a slight asymmetry as in the case of zero rotation.

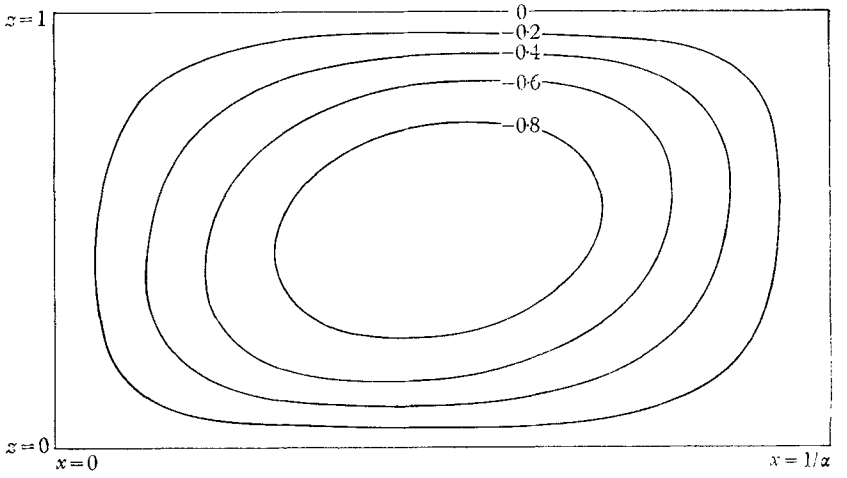

FIGURE 3. Streamlines for a typical case. The corresponding isotherms are shown in figure 4*a*. The flow is clockwise; i.e. cold fluid is convected downward and warm fluid upward.

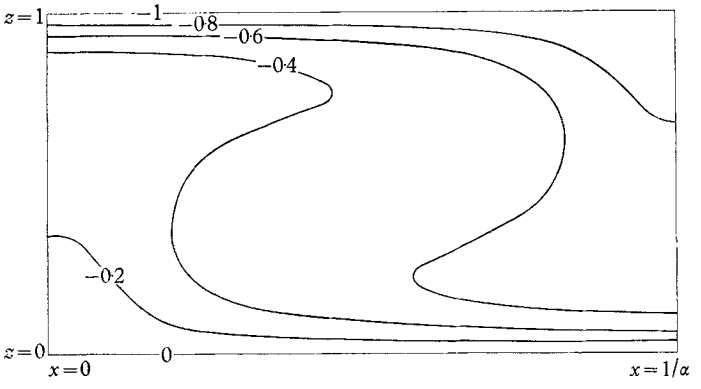

FIGURE 4*a*. Isotherm pattern for $\sigma = 6{\cdot}8$, $\mathscr{T}^2 = 10^3$, $R = 15{,}000$, $\alpha = 1{\cdot}181$. The anvil-shaped plumes are also typical of fluids with no rotation.

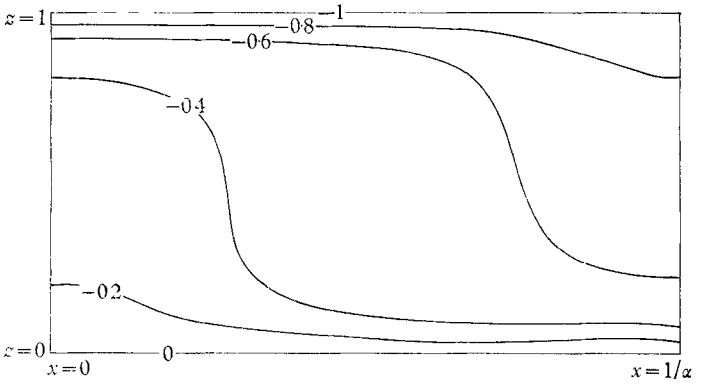

FIGURE 4*b*. Isotherm pattern for $\sigma = 6{\cdot}8$, $\mathscr{T}^2 = 10^5$, $R = 75{,}000$, $\alpha = 2{\cdot}746$. The strong constraining effect of rotation inhibits the formation of anvil-shaped plumes which exist for lower rotation rates.

Although the heat flux results show a certain similarity in behaviour as the Taylor number is increased, the isotherm patterns reflect the effect of rotating much more directly. For smaller values of $\mathscr{T}^2$ the thermal field resembles that of the non-rotating case. Anvil-shaped isotherms indicate that cold fluid sinks

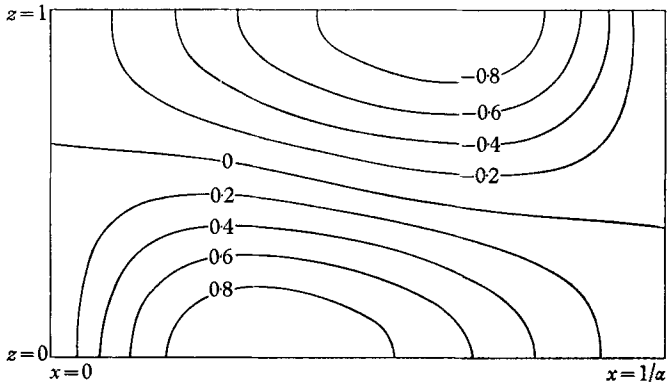

FIGURE 5*a*. Contour lines for the zonal velocity, v, associated with the isotherms of figure 4*a*. Strong non-linear effects give rise to a horizontal asymmetry but the pattern does not deviate too much from a symmetrical structure. Values of v are to be multiplied by 55·3.

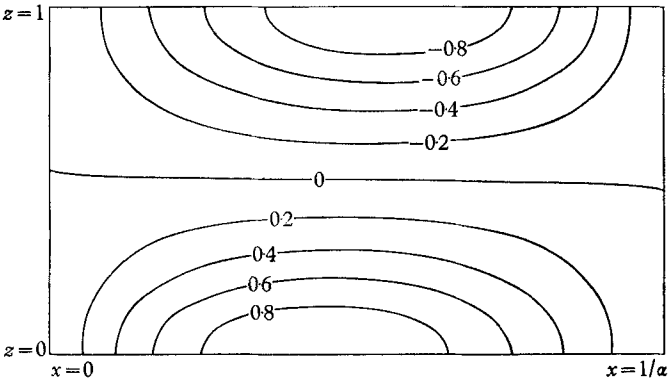

FIGURE 5*b*. Contour lines for the zonal velocity, v, associated with the isotherms of figure 4*b*. The larger constraint of rotation dominates the flow and the pattern is more symmetric than that of figure 5*a*. Values of v are to be multiplied by 96·4.

and spreads out close to the bottom boundary and plumes of warm fluid spread close to the top boundary (figure 4*a*). When $\mathscr{T}^2 = 10^5$ the horizontal spreading of the isotherms is inhibited as can be seen in figure 4*b*. For non-rotating or weakly rotating fluids the horizontal spreading of warm and cold plumes of fluid is uninhibited. However, strong rotation introduces a thermal wind balance where large horizontal temperature differences can be balanced by vertical shear of the zonal component of velocity. This balance becomes more and more pronounced as $\mathscr{T}^2$ increases and is the principal reason for the inhibition of convection (see I).

In figure 5*a* we show a pattern of contour lines for the zonal velocity, v, for the flow corresponding to the isotherm pattern of figure 4*a*. Flow very near R_c shows

a zonal velocity pattern which is simply antisymmetric with respect to the middle line $z = \frac{1}{2}$. Since the Taylor number is not very large for the case shown in figure 4*a* and since non-linear effects are quite strong (because $R \approx 9R_c$), the zonal velocities exhibit a skewness. The zonal velocity corresponding to the isotherms

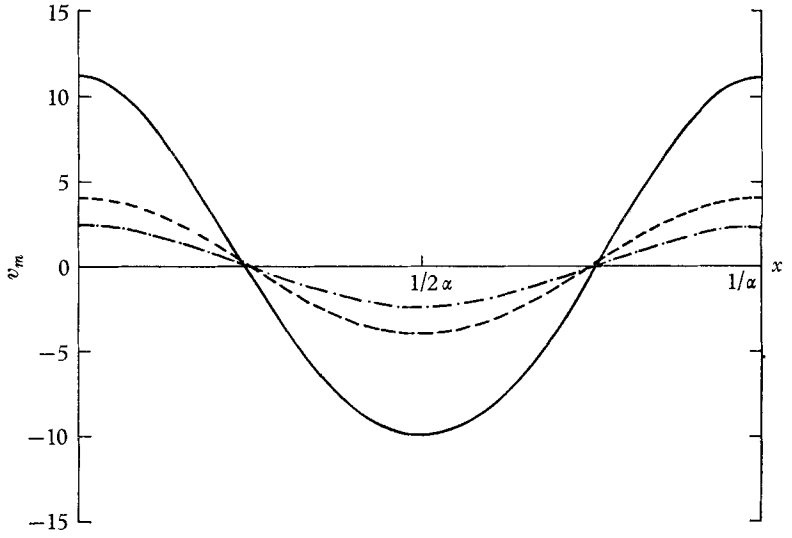

FIGURE 6. Graphs of v_m *vs.* x for the three cases noted in the diagram. Each curve is nearly antisymmetric in the right half-cell and left half-cell. This antisymmetry reflects the dominating role of rotation. Stronger non-linear effects destroy the symmetry as can be seen in figure 12. Note that the amplitudes of v_m are much smaller than those of v, indicating that the v fields are largely antisymmetric in z, i.e. that the flow is dominated by rotation. ——, $R = 15{,}000, \mathscr{T}^2 = 10^3$; – – – –, $R = 75{,}000, \mathscr{T}^2 = 10^5$; —·—· $R = 5000, \mathscr{T}^2 = 10^3$.

of figure 4*b* is shown in figure 5*b* and we note that the flow shows a more pronounced horizontal symmetry with little of the skewness of the previous case. This feature is due to the stronger constraint imposed by the larger Taylor number, with the horizontal temperature gradient more nearly balanced by the vertical shear of the zonal velocity. The amplitude of the zonal velocity is larger in the latter case.

The effect of the constraint is appreciated somewhat more if one looks at the vertical average of the zonal velocity (figure 6), i.e.

$$v_m = \int_0^1 v\,dz.$$

The quantity v_m essentially reflects the amount of zonal velocity which exists because of non-linearity. (At marginal stability v_m vanishes.) That part of v which contributes to the thermal wind, i.e. to balance the horizontal temperature gradient, has a vertical shear and does not contribute to v_m (in the linear solution we have imposed symmetry about $z = \frac{1}{2}$). Thus the ratio of the maximum amplitudes of v_m and v reflects the relative roles of non-linearity and the constraint of rotation. With that comparison in mind one notes that the constraining effect of rotation is much stronger in the case with $\mathscr{T}^2 = 10^5$ than with $\mathscr{T}^2 = 10^3$ at

the Rayleigh numbers shown. The graphs of v_m *vs.* x show that in each of the half cells v_m is nearly antisymmetric. This is a characteristic property of the flows for larger values of σ. We shall see that with $\sigma = 0{\cdot}2$ the flows in this range of Taylor number exhibit markedly different behaviour.

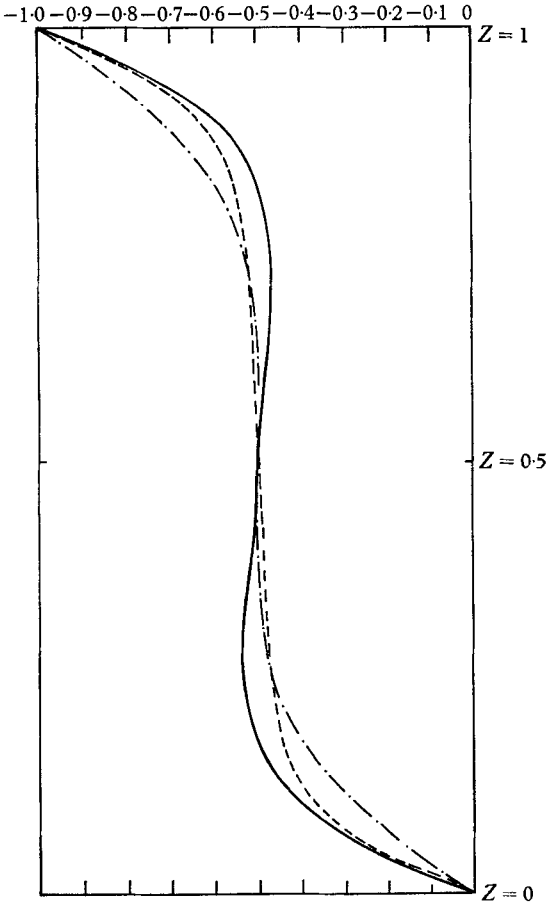

FIGURE 7. The horizontally averaged temperature, T_m, is plotted against the vertical co-ordinate for the three cases cited. The strong effect of the constraint for the case $\mathscr{T}^2 = 10^5$ is reflected in the slope of T_m, which is everywhere negative. In both of the cases for $\mathscr{T}^2 = 10^3$ the curves show a mean temperature gradient which is stable at mid-depth. ----, $R = 75{,}000, \mathscr{T}^2 = 10^5$; ——, $R = 15{,}000, \mathscr{T}^2 = 10^3$; —·—, $R = 5000, \mathscr{T}^2 = 10^3$.

We end the description of the dynamics of these cases for large Prandtl number with graphs of the horizontally averaged temperature, $T_m = \int_0^{1/\alpha} T\,dx$, *vs.* the vertical co-ordinate, z (figure 7). Recall that in the absence of convection the temperature distribution is linear in z. Hence, the deviation of T_m from a linear profile gives the degree of distortion of the mean temperature profile by non-linear effects. Qualitatively, the profiles reflect the convection of warm fluid upward and cold fluid downward with gradients sharpened near the top and

bottom boundaries. With $\mathscr{T}^2 = 10^3$ the mean temperature profiles resemble those of the non-rotating case. As R is increased a region with a stable mean temperature gradient appears in the middle of the layer. Such a region can potentially support oscillatory motions and may contribute to time-dependent behaviour for larger Rayleigh numbers. However, as we pointed out in II, this stable gradient may be associated with the restriction to two-dimensional flow and the concomitant inability of the fluid to generate three-dimensional instabilities.

Increasing the Taylor number alters the mean temperature profile by reducing the stable region in the middle of the fluid. Indeed, for $\mathscr{T}^2 = 10^5$ and $R = 75{,}000$ the mean temperature gradient is everywhere unstable. This feature is associated with the inhibition of plume formation by the strong constraint of rotation. Thus the convective inertia of the fluid is somewhat reduced by the rotation.

Because of the length of time required for the time integration of the systems with large σ no attempt was made to study the dependence of convection on horizontal wave-number, α.

Several features of Bénard convection in a rotating system with water which have been observed experimentally by Rossby are absent in this numerical study. At no time did our results exhibit finite-amplitude motions at subcritical Rayleigh numbers, although Rossby did observe unmistakable subcritical motions. Also in the present study Nu at a given Rayleigh number always decreased with increasing rotation rate. Rossby observed that at a given Rayleigh number the Nusselt number achieved a maximum value at finite Taylor numbers.

It seems likely that both of the foregoing features are associated with the rigid boundaries of the experiments. Rossby conjectured that rotation created Ekman layers near the boundaries and these enabled the fluid to behave somewhat like a system with free boundaries. Thus the relaxation of rigid boundary effects by the rotation may more than make up for the internal constraint brought about by the rotation. This possibility is, of course, not present in the free boundary system which we have explored. It marks one of the qualitative properties of convection which is completely missed by a free boundary investigation.

6. Convection in fluids with small Prandtl number

As we noted in the introduction, fluids with $\sigma < \sqrt{2}$ may be able to sustain finite-amplitude motions at subcritical values of the Rayleigh number. Table 2 shows minimum values of R and the corresponding α for which convection can be maintained for a fluid† with $\sigma = 0{\cdot}2$. Subscripts c and o respectively refer to the values derived by infinitesimal perturbation theory for steady convective modes (exchange of stabilities) and oscillatory (overstable) modes. According to analytical results with $K = 2$, finite-amplitude steady convection can exist at the values designated by R_f in the table. It should be noted that R_f is less than

† We had originally planned to study the behaviour of mercury ($\sigma = 0{\cdot}025$). However, the range of R for which finite-amplitude motions could occur extended so far below the critical values of linear theory that it was not possible to include a sufficient number of eigenmodes to get convergent results. It seems that one must attack this problem with a finite-difference analysis.

either R_o or R_c for Taylor numbers ranging up to just over $10^{\frac{9}{2}}$. For higher rotation rates these analytical results predict that $R_o < R_f$; hence there should be no finite-amplitude, subcritical, steady motions when $\mathscr{T}^2$ is sufficiently large.

$\log \mathscr{T}^2$	α_c	R_c	α_0	R_0	α_f	R_f
2	0·8256	826·3	0·7115	1591	0·7183	749·7
2·5	—	—	0·7208	1619	0·7183	837·3
3	1·181	1676	0·7475	1704	0·7183	1005
3·5	—	—	0·8143	1940	0·7183	1342
4	1·814	5377	0·9468	2522	0·7193	2059
4·5	—	—	1·153	3809	0·7183	3714
5	2·746	21309	1·429	6488	0·7183	7854

TABLE 2. Minimum values of R and corresponding wave-number, α, at which motions could be maintained when $\sigma = 0{\cdot}2$ for steady infinitesimal convection (subscript c), overstable infinitesimal convection (subscript o) and finite-amplitude steady convection (subscript f) for a range of Taylor number.

Because the pertinent values of R_f, R_o and R_c occur at different values of α it is necessary to include α as a separate parameter. We have used maximum heat flux as a criterion for selecting the preferred wave-number of the convecting fluid. An example of the type of study which was made is shown in table 3 where we list the Nusselt number for various values of α, K and R with $\mathscr{T}^2 = 10^3$. The numbers in parentheses heading each column give the pertinent values of K and α respectively.

For $\alpha = 0{\cdot}75$ we list values of Nu for $K = 4$, 6 and 8 in order to exhibit the convergence properties of the representation as a function of K. Thus up to $R = 4000$ a representation with $K = 8$ suffices. It is seen also that for $R \leqslant 4000$ maximum heat flux occurs for $\alpha = 0{\cdot}75$ (values enclosed in a box). For $R = 8000$, 20,000 and 30,000 the maxima (boxed numbers) occur at $\alpha = 0{\cdot}8$ although only for $R = 8000$ does the value of Nu derived with $K = 10$ satisfy our acceptability criterion (i e. differing by less than 1 % from the value of Nu with $K = 8$). However, from experience with the manner in which these systems converge with increasing K, it seems that at $R = 20{,}000$ the value of Nu with $K = 10$ very likely differs by less than 1 % from the value which one would derive with $K = 12$. We show Nu at $R = 30{,}000$ only to compare the results derived with $\alpha = 0{\cdot}8$ and $\alpha = 0{\cdot}85$. The actual numerical values at $R = 30{,}000$ are probably too low by more than 1 %. It is certainly conceivable that a calculation with $K = 12$ would show the maximum at $R = 3000$ to occur for $\alpha = 0{\cdot}85$.

The most important information exhibited in table 3 is, of course, the fact that finite-amplitude steady motions first occur in the range $1100 < R < 1200$. Thus, subcritical instabilities exist for a fluid with $\sigma = 0{\cdot}2$, since the minimum value of R according to linear stability theory occurs for oscillatory modes with $R_o = 1704$. It is important to note, however, that the minimum Rayleigh number at which these motions can exist is considerably above the value of $R_f = 1005$ derived analytically with $K = 2$ (see table 2). In none of the calculations were subcritical oscillatory motions found.

A similar listing of Nu for $\mathscr{T}^2 = 10^{\frac{7}{2}}$ is given in table 4, although we now include

R	$(8, 1/\sqrt{2})$	$(4, 0{\cdot}75)$	$(6, 0{\cdot}75)$	$(8, 0{\cdot}75)$	$(8, 0{\cdot}8)$	$(10, 0{\cdot}8)$	$(8, 0{\cdot}85)$	$(10, 0{\cdot}85$
1,100	1·0	1·0	1·0	1·0	1·0	1·0	1·0	1·0
1,200	1·665	1·768	1·698	1·682	1·676	—	1·644	—
1,500	2·137	2·200	2·158	2·142	2·131	—	2·104	—
1,800	2.432	2·482	2 452	2·437	2·428	—	2·403	—
2,000	2·590	2·632	2·610	2·595	2·586	—	2·565	—
4,000	—	—	3·599	3·594	3·591	—	3·576	—
8,000	—	—	4·631	4·715	4·720	4·726	4·708	4·716
20,000	6·365	—	5·819	6·385	6·392	6·593	6·373	6·590
30,000	—	—	—	—	—	7·484	—	7·483

3. Nusselt number as a function of α, K and R with $\mathscr{T}^2 = 10^3$ and $\sigma = 0{\cdot}2$. Pairs of numbers in parentheses heading each col
respectively the values of K and α. Values of maximum Nu at each R are enclosed in a box.

fewer columns since there is no new information on convergence as a function of K. We note that once again subcritical motions occur though the value of R at which these motions first occur ($1600 < R < 1700$) is not as far below the value for R_o (1940) as it is when $\mathscr{T}^2 = 10^3$. Also, maximum heat flux now occurs for $\alpha = 0{\cdot}8$ when $R \geqslant 1800$, although it is again possible that with $K = 12$ we would find the maximum at $R = 20{,}000$ to occur for $\alpha > 0{\cdot}8$.

R	(8, 0·75)	(8, 0·8)	(10, 0·8)	(10, 0·85)	(10, 0·9)
1,600	1·0	1·0	1·0	1·0	1·0
1,700	1·0	1·769	1·759	1·775	1·750
1,800	1·981	2·001	1·991	1·988	—
2,000	2·266	2·271	2·258	2·250	—
4,000	—	3·487	3·468	3·456	—
8,000	—	4·675	4·672	4·662	—
20,000	—	6·379	6·575	6·572	—

TABLE 4. Nusselt number as a function of α, K and R with $\mathscr{T}^2 = 10^{\frac{7}{2}}$ and $\sigma = 0{\cdot}2$. Heading each column in parentheses is the pair of values (K, α). Values of maximum Nu at each R are enclosed in a box.

Table 4 also shows that maximum heat flux at $R = 1700$ occurs for $\alpha = 0{\cdot}85$. Hence, as R is increased from the minimum value at which subcritical motions exist, the associated horizontal wave-number is first large then small then large again. This non-monotonic dependence of $Nu_{\max}$ on α is associated with another feature which we noted earlier and which was discussed in I; viz. at sufficiently large $\mathscr{T}^2$ no subcritical motions exist. Recall also that finite-amplitude motions can exist at subcritical R only because non-linear processes can overcome the constraint of rotation and that the associated horizontal wave-number is always smaller than the value given by linear theory. Hence, large α is associated with large $\mathscr{T}^2$ and small R. When finite amplitude motions can just be maintained, the effect of increasing $\mathscr{T}^2$ is to increase α. Thus, the minimum value of R at which motions can exist is raised and the corresponding value of α is also increased, being more dependent on $\mathscr{T}^2$.

This dependence of $Nu_{\max}$ on α for subcritical R is much more strikingly exhibited in table 5, which contains Nu as a function of α, K and R for $\mathscr{T}^2 = 10^4$. It is now seen that, in fact, finite-amplitude motions occur only for supercritical $R(> R_o)$ but (cf. table 2) steady motions still exist at values far below those given by linear theory ($R \ll R_c$). In this sense then the system still exhibits strong finite-amplitude behaviour at 'subcritical' values of R. Note that, as R goes from 3100 to 3500 to 4000 to 5000, $Nu_{\max}$ occurs at $\alpha = 0{\cdot}95$, 0·9, 0·85 and 0·8 respectively. For $R \geqslant 5000$ the preferred wave-number is still $\alpha = 0{\cdot}8$, although again we must admit the possibility that a larger representation may shift $Nu_{\max}$ toward larger values of α.

Since the wave-number for maximum Nu changes with R, it is certainly possible that a system with complete freedom of response would not settle down to a steady state at a single wave-number in the range $2522 \leqslant R \leqslant 5000$ but would

oscillate, perhaps irregularly, as non-linear effects would in turn dominate and be dominated by the rotational constraint. This is, of course, only speculation but the changing dependence of $Nu_{\max}$ on α strongly suggests possibilities other than a pure steady state.

R	(8, 0·8)	(10, 0·8)	(10, 0·85)	(10, 0·9)	(10, 0·95)	(10, 1·0)
2,500	1·0	1·0	1·0	1·0	1·0	1·0
2,700	—	—	—	*O*	*O*	*O*
3,000	*O*	*O*	*O*	*O*	*O*	*O*
3,100	—	*O*	2·055	2·140	2·162	2·155
3,500	2·642	2·574	2·601	2·608	2·599	2·577
4,000	3·025	2·955	2·964	2·958	—	—
5,000	—	3·478	3·476	—	—	—
8,000	4·521	4·480	4·472	—	—	—
20,000	6·341	6·516	6·513	—	—	—

TABLE 5. Nusselt number as a function of α, K and R with $\mathscr{T}^2 = 10^4$ and $\sigma = 0{\cdot}2$. Heading each column in parentheses is the pair of values (K, α). The letter O refers to a time-oscillatory behaviour. For the steady state, values of maximum Nu at each R are boxed.

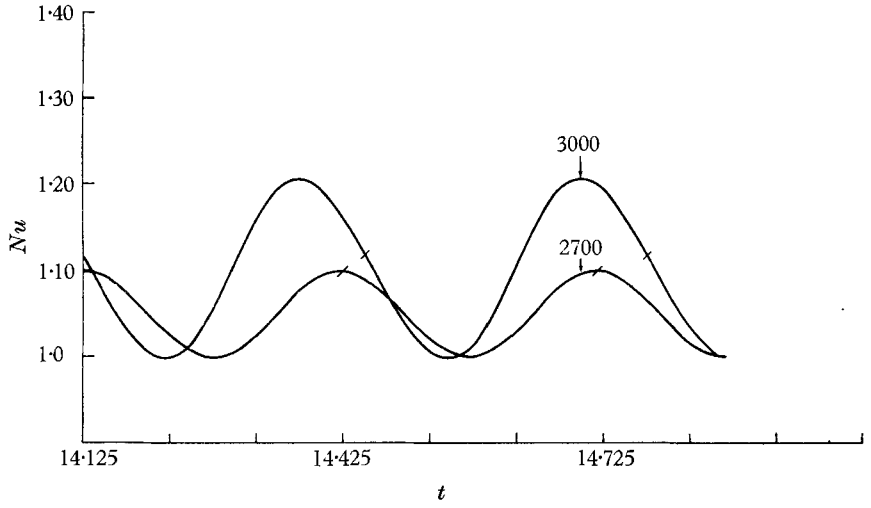

FIGURE 8. The periodic behaviour of the fluid with $\sigma = 0{\cdot}2$ is exhibited through the graphs for Nu *vs.* t when $\mathscr{T}^2 = 10^4$ and $\alpha = 0{\cdot}95$ for the two cases $R = 2700$ and $R = 3000$. The periods are marked as the lengths of abscissa between the two strokes on each curve. $K = 10$.

In figure 1 we show the onset of finite-amplitude instability as derived by the present calculations at $\mathscr{T}^2 = 10^3$, $10^{\frac{7}{2}}$ and 10^4 with $\sigma = 0{\cdot}2$. The small vertical lines delimit the ranges within which finite-amplitude steady motions could first be maintained. Thus, as we noted earlier, analytical results with $K = 2$ predict finite-amplitude instability for Taylor numbers up to a value slightly larger than $10^{\frac{9}{2}}$. But an accurate representation cuts the maximum $\mathscr{T}^2$ down to a value between $10^{\frac{7}{2}}$ and 10^4. One should keep in mind that finite-amplitude

instability in some sense still exists even beyond $\mathscr{T}^2 = 10^4$ because steady finite-amplitude motions occur for $R < R_c$. However, the initial onset of instability will take place according to linear stability theory for overstable motions.

Since overstable motions result when $\mathscr{T}^2 = 10^4$ and $2522 \leqslant R \leqslant 3100$, we can investigate the oscillatory nature of these motions by examining the dependence of Nu on t when the system has settled to a periodic behaviour between fixed limits. Graphs of Nu *vs.* t are exhibited in figure 8 for $R = 2700$ and $R = 3000$ with $\alpha = 0{\cdot}95$ and $K = 10$. It was necessary to carry the calculation to $t > 13$ (t is non-dimensionalized with respect to d/κ) when the calculation was made using the steady finite-amplitude solution with $K = 2$ as initial conditions. Since Nu depends on the correlation of w and T, the period exhibited by Nu is half of the period of either w or T when R is sufficiently close to R_c. For $R = 3000$ there is some distortion of Nu *vs.* t from a simple sinusoidal oscillation as can be seen by the steeper part of the curve for increasing Nu. However, we can still use the period as a measure of the half-period for w or T because the major contribution to the heat flux comes from the $\cos(\pi\alpha x)\sin(\pi z)$ component. According to linear stability theory the period for $\mathscr{T}^2 = 10^4$ and $\sigma = 0{\cdot}2$ occurs at $R = 2522$ and is approximately 0·558 non-dimensional units. At $R = 2700$ our results give a period of 0·590 and at $R = 3000$ the period is 0·650 but with some skewness in the curve. Hence, non-linear effects increase the period or decrease the frequency. This behaviour was also observed by Rossby for low values of $\mathscr{T}^2$.

We also observe that the heat flux for these oscillatory modes is considerably less than the heat fluxes which exist when steady motions are possible at subcritical R. Thus at $R = 3000$ Nu oscillates between values of 1·0 and 1·205. At $R = 3100$ where steady motions can be maintained $Nu = 2{\cdot}162$. Such large quantitative differences in Nu between oscillatory and non-oscillatory motions were also observed experimentally by Rossby.

Contour maps of the field variables for the steady subcritical flows which exist with $\sigma = 0{\cdot}2$ show some features which directly reflect the strong non-linear character of the flow. Contour maps of ψ in the (x, z)-plane are very similar to those of the non-rotating system (see II) and are not shown here.

The isotherm patterns also show the effect of stronger non-linear behaviour. Figure 9*a* is a map of isotherms for the case $\alpha = 0{\cdot}75$, $\mathscr{T}^2 = 10^3$, $R = 1200$, i.e. near the minimum value of R for which motions exist. It is seen that, even though there is no mushroom structure to the isotherms, warm and cold plumes of fluid extend quite far from the lower and upper boundaries respectively. Figure 9*b* gives equivalent results for $\alpha = 0{\cdot}85$, $\mathscr{T}^2 = 10^4$, $R = 4000$, i.e. for a value of R considerably larger than the minimum, and shows a mushroom-like pattern similar to that of figure 4*a*. Cold and warm plumes of fluid again extend deeper into the system from the upper and lower boundaries.

Shown in figure 10 are the two graphs of the horizontally averaged temperature field corresponding to the isotherm patterns of figures 9*a* and 9*b*. For $R = 1200$, $\mathscr{T}^2 = 10^3$ the mean temperature deviates relatively little from the linear profile whereas for $R = 4000$, $\mathscr{T}^2 = 10^4$ the profile is similar to those for large σ. Hence, in the lower range of Rayleigh number the cause of subcritical finite-amplitude motions must be more strongly associated with some property

other than the temperature field because the latter shows little of the distortion generally associated with strongly non-linear convection.

In I and in an earlier paper (Veronis 1959) it was shown that finite-amplitude

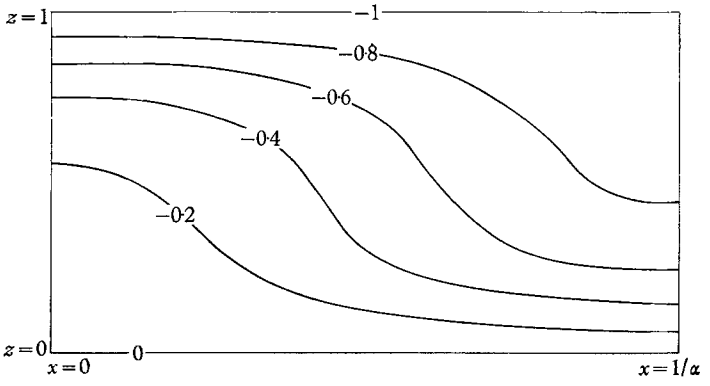

FIGURE 9*a*. The isotherms for $\sigma = 0{\cdot}2$, $\alpha = 0{\cdot}75$, $\mathscr{T}^2 = 10^3$ and $R = 1200$. Motion can just be maintained at this value of R and the temperature field shows little of the distortion characteristic of flows at larger R. Note, however, the deep penetration of hot and cold plumes from the lower and upper boundaries respectively.

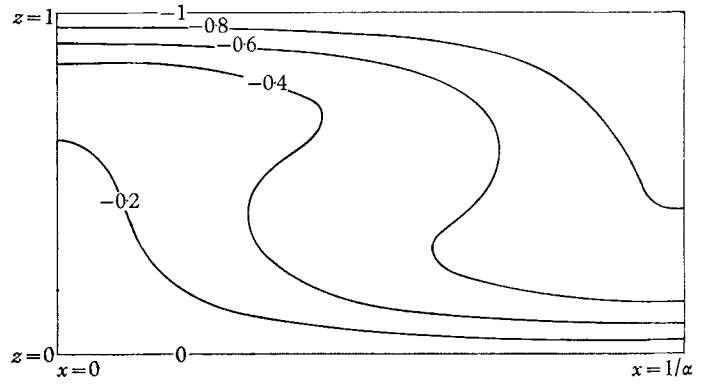

FIGURE 9*b*. Isotherms for $\sigma = 0{\cdot}2$, $\alpha = 0{\cdot}85$, $\mathscr{T}^2 = 10^4$ and $R = 4000$. The fluid is convecting much more strongly than that in figure 9*a*. This behaviour is exhibited by the formation of anvil-shaped isotherms just as in non-rotating fluids.

instability may occur at subcritical Rayleigh numbers because non-linear processes can offset the constraining effect of rotation. The more of the constraint which is balanced by inertial effects, the less is available to balance the horizontal temperature gradients which occur and the fluid may therefore exhibit behaviour closer to that of the non-rotating system with flow down the pressure gradient. The constraint manifests itself principally through the zonal velocity, v. Figures 11*a* and 11*b* show how much the present zonal velocities differ from those obtained with $\sigma = 6{\cdot}8$. The nearly symmetric horizontal structure of v about the mid-point of the half cell in figures 5*a* and 5*b* is now completely absent and is replaced by a diagonal antisymmetry. For $\sigma = 6{\cdot}8$ the zonal velocity is

essentially antisymmetric about the mid-level. Such a structure is a reflexion of the thermal wind balance $\partial v/\partial z \propto \partial T/\partial x$. The patterns of 11*a* and 11*b* imply that v_m, the vertical average of the zonal velocity, has a relatively large amplitude. It was pointed out earlier than the ratio of the amplitudes of v_m to v reflects the intensity of non-linear processes.

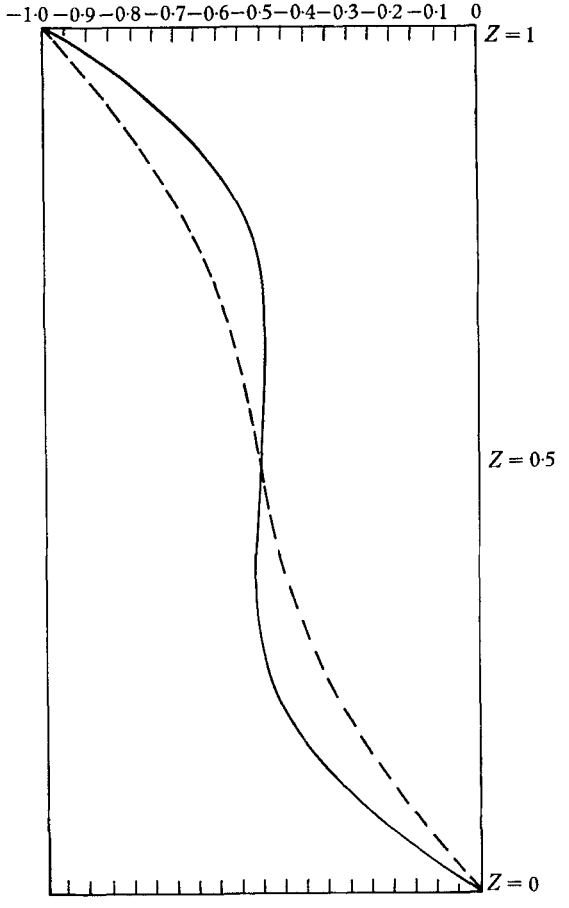

FIGURE 10. T_m *vs.* z when $\sigma = 0{\cdot}2$ for the two cases shown in figures 9*a* and 9*b*. The interior of the fluid shows a relatively small departure from the linear temperature gradient in the case with $R = 1200$ and $\mathscr{T}^2 = 10^3$. When $\mathscr{T}^2 = 10^4$ and $R = 4000$ the curve for T_m looks more like that for the non-rotating fluid. —, $\mathscr{T}^2 = 10^4$, $R = 4000$, $\alpha = 0{\cdot}85$; — —, $\mathscr{T}^2 = 10^3$, $R = 1200$, $\alpha = 0{\cdot}75$.

Further qualitative evidence of a strongly non-linear behaviour is exhibited by the graphs of v_m *vs.* x as shown in figure 12. The amplitudes of v_m are comparable to the corresponding amplitudes of v. Furthermore, the near antisymmetries which are present in figure 6 in the left and right half-cells are now absent. There is a more intense concentration of positive mean zonal velocity near the lateral boundaries of the cell and a broader region of negative zonal velocity with smaller amplitude in the mid-area. Both figures 11 and 12 show some of the irregularity of the Fourier representation. Recall that for these subcritical flows it is necessary

to use a large number of terms to derive a representation which is even marginally accurate.

In his experimental studies with mercury Rossby has observed subcritical motions as we predict here. However, he has not observed steady motions in

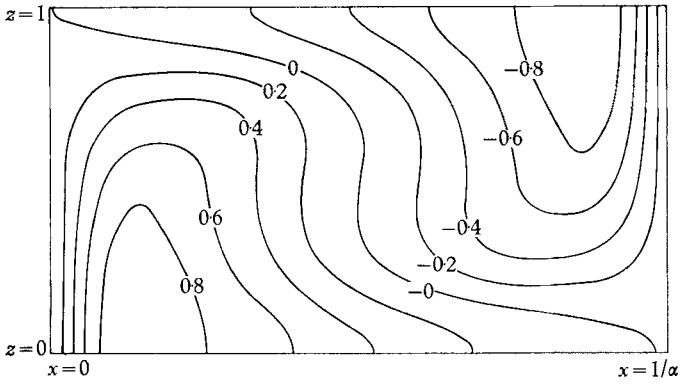

FIGURE 11*a*. Contours of v for $\sigma = 0{\cdot}2$, $\mathscr{T}^2 = 10^3$, $R = 1200$. The nearly horizontal symmetry characteristic of fluids with large σ is now entirely absent and a strong shift of maximum and minimum velocities toward the lateral boundaries has taken place. This property is characteristic of cases in which a finite-amplitude instability can occur. Values of v are to be multiplied by 4·37.

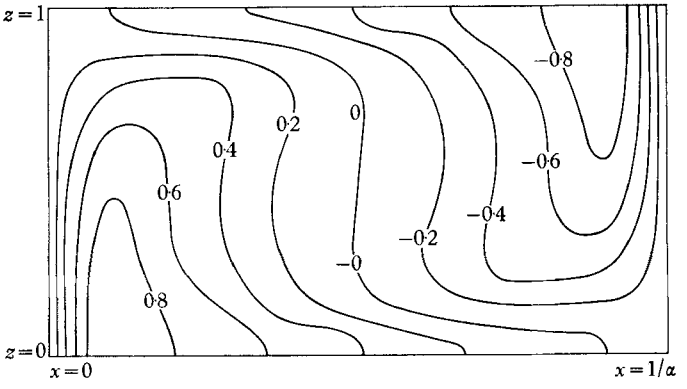

FIGURE 11*b*. Contours of v for $\sigma = 0{\cdot}2$, $\mathscr{T}^2 = 10^4$, $R = 4000$. The behaviour is similar to that of figure 11*a* though more intense. Values of v are to be multiplied by 11·7.

any of his experiments with mercury. Indeed, even when the fluid is not rotating, the observed motions are unsteady. However, one can distinguish experimentally between the aperiodic unsteady motions which exist when theory predicts steady motions and the periodic oscillatory motions corresponding to overstable modes. Rossby observes subcritical, aperiodic transient motions at lower rotation rates. When $\mathscr{T}^2$ is increased, subcritical overstable modes occur. At sufficiently high rotation rates mercury first becomes unstable to overstable modes as predicted by linear theory.

Hence, it appears again that the present study of a two-dimensional fluid with free boundaries misses some of the observed behaviour even at relatively moderate Rayleigh numbers. It is conceivable (though it appears to me to be unlikely)

that a fluid with $\sigma = 0{\cdot}2$ behaves in a fashion qualitatively different from mercury. The discrepancy is probably due to the different boundary conditions. However, it is not obvious that one can put forth a simple argument similar to

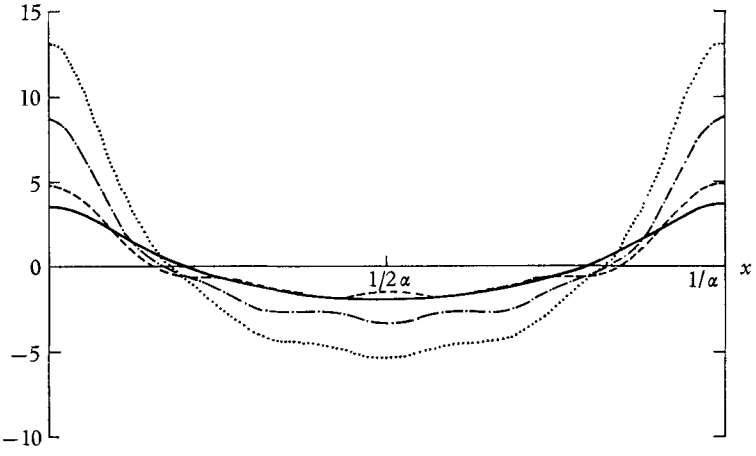

FIGURE 12. v_m *vs.* x for the four cases cited. Note the concentration of larger amplitudes toward the lateral boundaries of the cell. The symmetry properties of these fields are quite different from those shown in figure 6. Note too that the amplitudes of v_m are comparable to those of v; thus inertial effects are more important than they are when $\sigma = 6{\cdot}8$. ——, $\mathscr{T}^2 = 10^3$, $R = 1200$, $\alpha = 0{\cdot}75$; – – – –, $\mathscr{T}^2 = 10^3$, $R = 4000$, $\alpha = 0{\cdot}8$; —·—·, $\mathscr{T}^2 = 10^{3\frac{1}{2}}$, $R = 4000$, $\alpha = 0{\cdot}85$; ....., $\mathscr{T} = 10^4$, $R = 4000$, $\alpha = 0{\cdot}85$.

the one proposed to explain the discrepancy between theory and experiment for water (relaxation of rigid boundary conditions because of rotation) in order to explain the present lack of agreement. Partly the reason for this is that several processes are combined when time-dependence is possible and it is difficult to delimit the role of each. It is very possible that the explanation may involve non-linear interactions of the effects of transient behaviour with the effects of the boundaries.

Mrs J. Webster programmed some of the subroutines and Messrs. P. Schneck, C. Blomquist and A. Rosati ran the progams. Dr R. Jastron generously made available the computing facilities of the NASA Institute for Space Studies in New York. The National Science Foundation supported the research through grants GP. 4321 and GA. 872. I am grateful to these individuals and institutions for their help.

REFERENCES

CHANDRASEKHAR, S. 1961 *Hydrodynamic and Hydromagnetic Stability.* Oxford: Clarendon Press.

ROSSBY, H. T. 1966 An experimental study of Bénard convection with and without rotation. Ph.D. Thesis, Mass. Inst. Techn.

VERONIS, G. 1959 Cellular convection with finite amplitude in a rotating fluid. *J. Fluid Mech.* **5**, 401.

VERONIS, G. 1966 I. Motions at subcritical values of the Rayleigh number in a rotating fluid. *J. Fluid Mech.* **24**, 545.

VERONIS, G. 1966 II. Large-amplitude Bénard convection. *J. Fluid Mech.* **26**, 49.